Mössbauer study on epitaxial Co x Fe4− x N films grown by molecular beam epitaxy

Keita Ito, Tatsunori Sanai, Yoko Yasutomi, Toshiki Gushi, Kaoru Toko, Hideto Yanagihara, Masakiyo Tsunoda, Eiji Kita, and Takashi Suemasu

Articles you may be interested in

X-ray magnetic circular dichroism for Co x Fe4− x N (x=0, 3, 4) films grown by molecular beam epitaxy
J. Appl. Phys. **115**, 17C712 (2014); 10.1063/1.4862517

Perpendicular magnetic anisotropy in CoFe2O4(001) films epitaxially grown on MgO(001)
J. Appl. Phys. **109**, 07C122 (2011); 10.1063/1.3566079

Adsorption-controlled molecular-beam epitaxial growth of Bi Fe O 3
Appl. Phys. Lett. **91**, 071922 (2007); 10.1063/1.2767771

Neutron diffraction and Mössbauer studies of CoAl x Fe 2−x O 4
J. Appl. Phys. **93**, 7504 (2003); 10.1063/1.1557955

Synthesis of epitaxial films of Fe 3 O 4 and α -Fe 2 O 3 with various low-index orientations by oxygen-plasma-assisted molecular beam epitaxy
J. Vac. Sci. Technol. A **15**, 332 (1997); 10.1116/1.580488

Mössbauer study on epitaxial Co$_x$Fe$_{4-x}$N films grown by molecular beam epitaxy

Keita Ito,[1,2,3,a)] Tatsunori Sanai,[1] Yoko Yasutomi,[1] Toshiki Gushi,[1] Kaoru Toko,[1] Hideto Yanagihara,[1] Masakiyo Tsunoda,[3] Eiji Kita,[1] and Takashi Suemasu[1]

[1]*Institute of Applied Physics, Graduate School of Pure and Applied Sciences, University of Tsukuba, 1-1-1 Tennodai, Tsukuba, Ibaraki 305-8573, Japan*
[2]*Japan Society for the Promotion of Science (JSPS), 5-3-1 Kojimachi, Chiyoda-ku, Tokyo 102-0083, Japan*
[3]*Department of Electronic Engineering, Graduate School of Engineering, Tohoku University, 6-6-05 Aobayama, Sendai 980-8579, Japan*

We prepared Co$_x$Fe$_{4-x}$N ($x = 0, 1, 3$) films on SrTiO$_3$(STO)(001) substrates by molecular beam epitaxy. The epitaxial relationship with Co$_x$Fe$_{4-x}$N[100](001) || STO[100](001) was confirmed by ω-2θ (out-of-plane) and ϕ-$2\theta_\chi$ (in-plane) x-ray diffraction (XRD) measurements. The degree of order of atoms (S) in the Co$_x$Fe$_{4-x}$N films was estimated to be ∼0.5 by the peak intensity ratio of Co$_x$Fe$_{4-x}$N(100) (superlattice diffraction line) to (400) (fundamental diffraction line) in the ϕ-$2\theta_\chi$ XRD patterns. Conversion electron Mössbauer spectroscopy studies for the Co$_x$Fe$_{4-x}$N films revealed that some N atoms are located at interstitial sites between the two nearest corner sites in the Co$_x$Fe$_{4-x}$N films, and/or Fe atoms are located at both the corner and face-centered sites in the CoFe$_3$N and Co$_3$FeN films. In order to realize high spin-polarized Co$_x$Fe$_{4-x}$N films having large S, further optimization of growth condition is required to prevent the site-disorders. © 2015 AIP Publishing LLC. [http://dx.doi.org/10.1063/1.4914342]

I. INTRODUCTION

In order to realize high performance spintronics devices, high spin-polarized ferromagnetic materials are demanded. Co$_x$Fe$_{4-x}$N are promising ferromagnetic materials for spintronics devices due to their large spin-polarization of density of states (D) at the Fermi level (E_F): $P_D = [D_\uparrow(E_F) - D_\downarrow(E_F)]/[D_\uparrow(E_F) + D_\downarrow(E_F)]$.[1–3] Figure 1 shows the lattice structure of anti-perovskite Co$_x$Fe$_{4-x}$N. Kokado *et al.* calculated P_D in Fe$_4$N to be −0.60 by the first-principles calculation.[1] They also simulated the spin dependent electrical conductivity (σ) in Fe$_4$N by a combination of the first-principles, tight-binding calculations, and Kubo formula, and deduced its spin-polarization of σ: $P_\sigma = (\sigma_\uparrow - \sigma_\downarrow)/(\sigma_\uparrow + \sigma_\downarrow)$, to be −1.0.[1] Imai *et al.* calculated P_D in Co$_4$N to be −0.88 by the first-principles calculation.[2] However, the deficiency of the N atoms was reported in Co$_4$N.[4] Takahashi *et al.* reported that the Co$_3$FeN is expected to have larger $|P_D|$ of 0.75 ($P_D < 0$) than that of Fe$_4$N when Fe atoms are located at the corner (I) sites, and Co atoms at the face-centered (II) sites in the anti-perovskite unit cell.[3] There are no reports thus far on P_σ in Co$_3$FeN. However, we believe that Co$_3$FeN could be superior to Fe$_4$N as the spin injection electrode of spintronics devices because of its larger $|P_D|$ than that of Fe$_4$N. We have succeeded in growing epitaxial Co$_x$Fe$_{4-x}$N films on SrTiO$_3$(STO)(001) substrates by molecular beam epitaxy (MBE).[5–7] X-ray magnetic circular dichroism measurements were performed on the epitaxially grown Co$_3$FeN film, and spin and orbital magnetic moments per an Fe and Co atom were evaluated and compared them with those deduced by

the first-principles calculation.[8,9] It was suggested that Fe and Co atoms in the Co$_3$FeN film are located at both I and II sites, which indicates that the ideal lattice structure without the Fe-Co site disorder supposed in Ref. 3 was not realized.[8,9] In addition, the first-principles calculation revealed that the Fe-Co site disorder reduces $|P_D|$ in Co$_3$FeN.[8] Recently, Kabara and Tsunoda reported the temperature dependence of the anisotropic magnetoresistance in Fe$_4$N and showed that the degree of order of atoms (S) in the anti-perovskite lattice affects the electronic structure of Fe$_4$N.[10] Thus, the magnitude of S in Co$_x$Fe$_{4-x}$N films affects their $|P_D|$, and a large S value is desirable. In this study, we evaluated S values in Co$_x$Fe$_{4-x}$N films by x-ray diffraction (XRD) measurements and compared them with the results of conversion electron Mössbauer spectroscopy (CEMS). The CEMS measurement
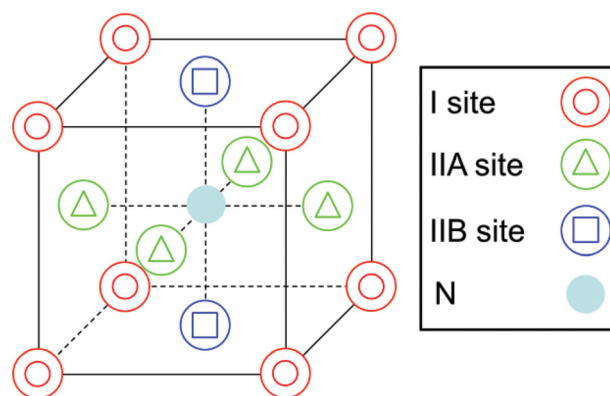

FIG. 1. Lattice structure of anti-perovskite type ferromagnetic nitrides. II sites are distinguished by IIA and IIB sites due to the orientation of the internal magnetic field.

a)Electronic mail: keita.ito.729@gmail.com

can directly provide the occupation of Fe sites and the site-disorders in $Co_xFe_{4-x}N$. There are many reports on the Mössbauer studies for Fe_4N.[11–14] However, there have been no reports thus far on the Mössbauer measurements for Fe atoms in the epitaxially grown $Co_xFe_{4-x}N$ films.

II. EXPERIMENTAL METHODS

We grew 19-nm-thick Fe_4N (sample A), 25-nm-thick $CoFe_3N$ (sample B), and 74-nm-thick Co_3FeN films (sample C) on STO(001) substrates by MBE, supplying an ^{57}Fe enriched ($\sim20\%$) solid iron, a solid cobalt, and a radio-frequency (RF) nitrogen plasma, simultaneously at 450 °C. The total supply of Fe and Co atoms, the flow rate of N_2 gas, and RF plasma input power were fixed. The grown layer of sample C (small Fe amount) was thicker than those of samples A and B to obtain enough CEMS signals for the analysis. The crystalline qualities of the $Co_xFe_{4-x}N$ films were characterized by ω–2θ (out-of-plane) and ϕ–$2\theta_\chi$ (in-plane) XRD measurements using Cu-$K\alpha$ x-rays at room temperature (RT). In the ϕ–$2\theta_\chi$ XRD measurements, the scattering vector was aligned along the in-plane STO[100] direction, and Ge(220) single crystals to make the x-rays monochromatic were not used in order to observe the weak diffraction peak of $Co_xFe_{4-x}N$(100). The peaks labeled with # indicate the diffractions caused by the Cu-$K\beta$ or W-$L\alpha$ x-rays. S values of samples A–C were evaluated by substituting I_{hkl}^{obs} and I_{hkl}^{cal} of the $Co_xFe_{4-x}N$(100) and (400) diffraction lines in the ϕ–$2\theta_\chi$ XRD patterns into[10]

$$S = \sqrt{\frac{I_{100}^{obs}/I_{400}^{obs}}{I_{100}^{cal}/I_{400}^{cal}}}. \quad (1)$$

Here, I_{hkl}^{obs} is the experimentally observed diffraction peak intensity of (hkl), and I_{hkl}^{cal} is the theoretical one calculated by commercially available software, CaRIne Crystallography 3.1. The diffraction of $Co_xFe_{4-x}N$(100) is a superlattice line, which stands out when N, Fe, and Co atoms are ordered, while that of $Co_xFe_{4-x}N$(400) is a fundamental line. In this work, we used the $Co_xFe_{4-x}N$(400) diffraction instead of $Co_xFe_{4-x}N$(200), differently from Ref. 10, in order to distinguish I_{hkl}^{obs} of the films clearly from that of the STO. For I_{hkl}^{cal} values of $CoFe_3N$ (Co_3FeN), we assumed that the Fe (Co) atoms are located at face-centered sites. The surface morphologies of samples A–C were observed by an atomic force microscope (AFM). CEMS measurements for the $Co_xFe_{4-x}N$ films were performed at RT. The velocity and isomer shift were calibrated using a standard spectrum of α-Fe. Obtained CEMS spectra were analyzed using the commercially available fitting software, MössWinn 4.0.

III. RESULTS AND DISCUSSION

Figures 2(a)–2(c) display the ω–2θ XRD patterns of samples A–C, respectively. The diffraction lines corresponding to $Co_xFe_{4-x}N$(001), (002), and (004) were observed for all the samples. Figures 3(a)–3(c) display the ϕ–$2\theta_\chi$ XRD patterns of samples A–C, respectively. $Co_xFe_{4-x}N$(100), (200), and (400) diffraction lines were obtained for all the
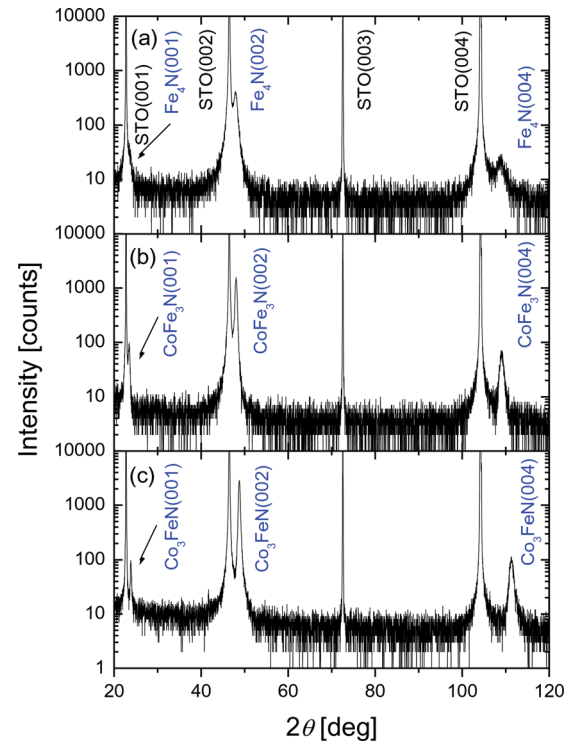

FIG. 2. ω-2θ (out-of-plane) XRD patterns of the (a) Fe_4N, (b) $CoFe_3N$, and (c) Co_3FeN films.

samples. Thereby, $Co_xFe_{4-x}N$ ($x = 0, 1, 3$) films were epitaxially grown on STO(001) substrates with the relationship of $Co_xFe_{4-x}N$[100](001) || STO[100](001). By the curve fitting to the ϕ–$2\theta_\chi$ XRD patterns shown in Fig. 3 with the Lorenz function, we deduced I_{100}^{obs} and I_{400}^{obs} for samples A–C, and

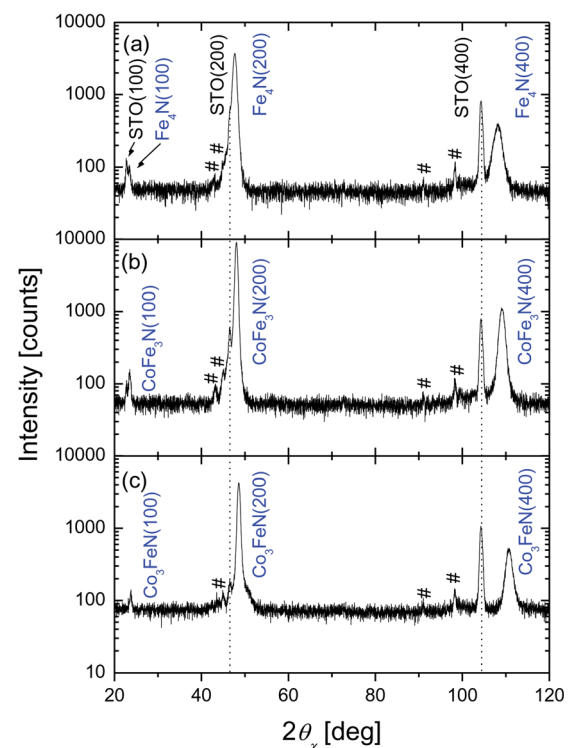FIG. 3. ϕ-$2\theta_\chi$ (in-plane) XRD patterns of the (a) Fe_4N, (b) $CoFe_3N$, and (c) Co_3FeN films. The scattering vector was set along the STO[100] direction.
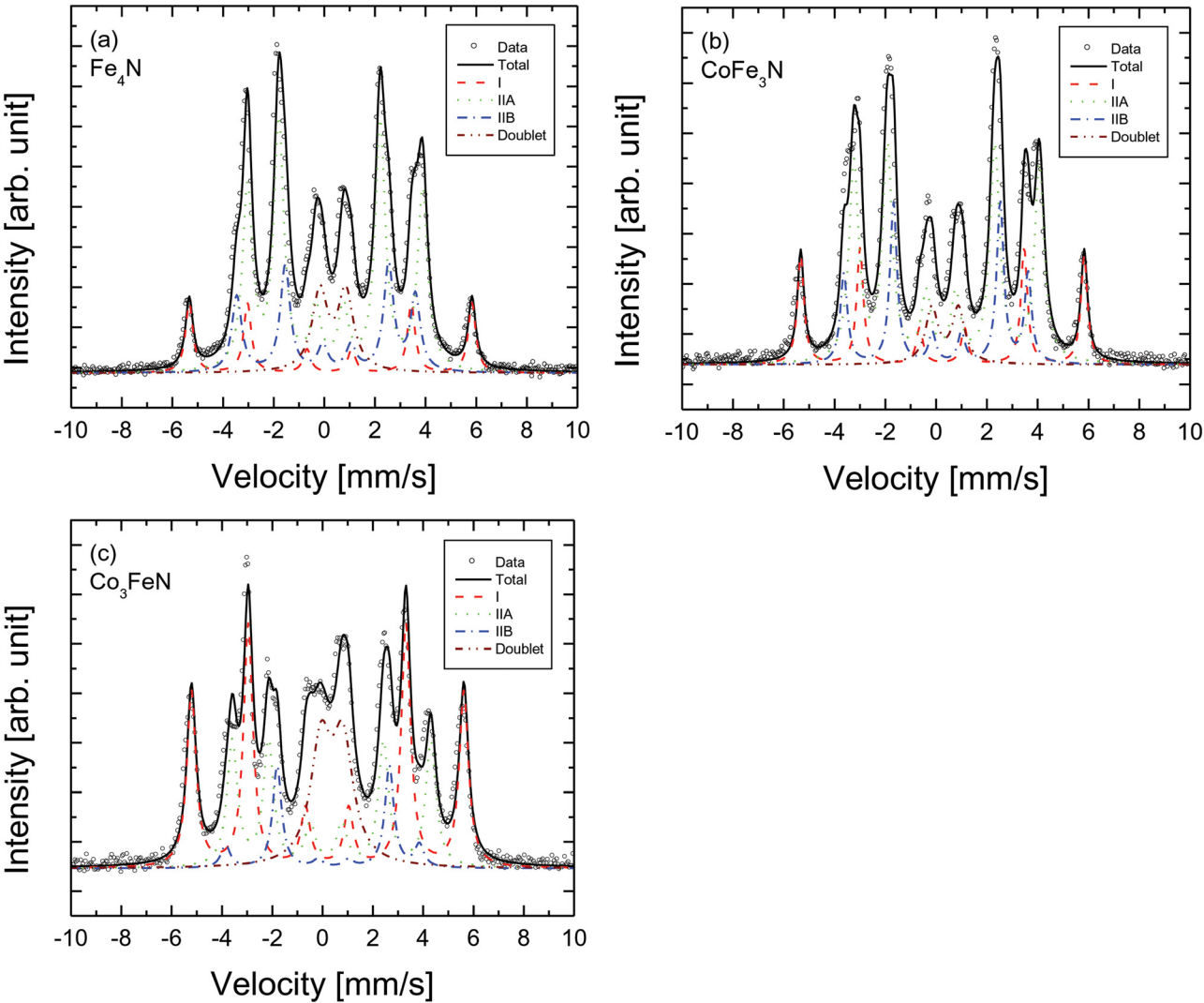
FIG. 4. Mössbauer spectra and curve fitting results of the (a) Fe_4N, (b) $CoFe_3N$, and (c) Co_3FeN films. Open dots and black solid lines show the experimental data and total fitting curves, respectively. Red, green, blue, and brown lines correspond to the components of I, IIA, IIB sites, and doublet, respectively.

substituted these values and I_{100}^{cal} and I_{400}^{cal} into Eq. (1). S were deduced to be 0.56, 0.57, and 0.47, respectively, for samples A–C. As to sample A, Fe_4N, this value ($S = 0.56$) is smaller than $S = 0.93$ reported on the Fe_4N film formed by a sputtering technique on MgO(001) after the post annealing at 300 °C.[10] This indicates that some N atoms are not located at the body center of cube,[10] and/or there are excess N atoms inserted between the two nearest I sites in the Fe_4N layer (sample A). $S = 0.47$ in the Co_3FeN layer (sample C) is smaller than $S = 0.57$ in the $CoFe_3N$ layer (sample B). Increase of the Co amount in $Co_xFe_{4-x}N$ might promote the deficiency of the N atoms and reduce its S because of the low stability of N atoms in Co_4N.[4]

Figures 4(a)–4(c) show the CEMS spectra of samples A–C, respectively. Table I summarizes the Mössbauer parameters of samples A–C deduced by the curve fitting to the CEMS spectra shown in Fig. 4. Obtained CEMS spectra were decomposed into three ferromagnetic components and one paramagnetic component. We consider that the paramagnetic component is attributed to the surface oxidized layer. The relative area of the paramagnetic component in sample C was approximately twice as large as those of samples A

and B. The root-mean-square (RMS) values of the surface roughness of samples A–C were found to be 1.2, 0.34, and 14 nm, respectively, by AFM measurements. The surface

TABLE I. Mössbauer parameters of the $Co_xFe_{4-x}N$ films deduced by the curve fitting to the Mössbauer spectra shown in Fig. 4. H, δ, ε, and R. A. are the hyperfine field, isomer shift, quadrupole splitting, and relative area, respectively.

Compounds	Components	H [T]	δ [mm/s]	ε [mm/s]	R. A. [%]
Fe_4N	I	34.71	0.22	0.05	13.02
	IIA	21.50	0.31	0.22	52.30
	IIB	21.92	0.28	−0.43	21.78
	Doublet	…	0.33	1.02	12.89
$CoFe_3N$	I	34.69	0.24	0.01	19.07
	IIA	22.70	0.30	0.22	51.38
	IIB	22.55	0.21	−0.43	21.97
	Doublet	…	0.35	1.05	7.58
Co_3FeN	I	33.65	0.19	0.02	39.99
	IIA	24.53	0.25	0.22	27.24
	IIB	23.94	0.21	−0.43	10.81
	Doublet	…	0.37	0.87	21.97

roughness of sample C is quite large and thus its surface area became much larger than those of samples A and B. The magnitude of relative area of the paramagnetic component was increased with increasing the RMS values of the nitride layers because the large surface area prompts oxidation of the film. Thus, we concluded that the paramagnetic doublet is due to the surface oxidation. The values of a hyperfine field, an isomer shift, and a quadrupole splitting of sample A were in good agreement with those reported.[11] However, the relative area ratio of I:II sites was not an ideal value of 1:3, but 0.53:3. The in-plane lattice parameter of the Fe_4N layer in sample A deduced from Fig. 3(a) was 0.3812 nm and is almost the same as that of the bulk value (0.3795 nm).[15] Thus, we believe that this extremely small occupation value for I sites is not attributed to Fe vacancies, but to the excess insertion and/or site-disorder of the N atoms since I sites are equivalent to II sites when the N atoms are located at interstitial sites between the two nearest I sites. This result is consistent with the medium degree of S in sample A. The $3d$ atoms located at I sites of $Co_xFe_{4-x}N$ have the nearly half-metallic feature.[17,18] Thereby, the improvement of S and the prevention of the extinction of I sites lead to the high spin-polarization in $Co_xFe_{4-x}N$. The results of CEMS measurements for samples B and C indicated that Fe atoms in samples B and C are located at both I and II sites and/or there is the site-disorder of the N atoms. This is consistent with our previous report.[8,9] This trend is also theoretically supported by the first-principles calculation, which shows that Co atoms tend to occupy both the I and II sites in $Co_xFe_{4-x}N$ from the view point of total energy.[16] In order to obtain high spin-polarized $Co_xFe_{4-x}N$, optimization of the growth conditions is required to prevent the site-disorders. We believe that the optimization of the supply rate of N atoms during growth and the post-annealing technique[10] are predictably effective.

IV. SUMMARY

We evaluated S values in the epitaxially grown Fe_4N, $CoFe_3N$, and Co_3FeN films on STO(001) substrates by MBE from the XRD measurements. The medium degree of the site-disorders ($S \sim 0.5$) was confirmed for all the samples. CEMS measurements revealed that some N atoms are located at interstitial sites between the two nearest I sites in the $Co_xFe_{4-x}N$ films, and/or Fe atoms are located at both I and II sites in the $CoFe_3N$ and Co_3FeN films. They are consistent with the medium degree of the site-disorder of atoms confirmed from the XRD measurements. Further optimization of the growth conditions is required to realize the high spin-polarized $Co_xFe_{4-x}N$.

[1] S. Kokado, N. Fujima, K. Harigaya, H. Shimizu, and A. Sakuma, Phys. Rev. B **73**, 172410 (2006).

[2] Y. Imai, Y. Takahashi, and T. Kumagai, J. Magn. Magn. Mater. **322**, 2665 (2010).

[3] Y. Takahashi, Y. Imai, and T. Kumagai, J. Magn. Magn. Mater. **323**, 2941 (2011).

[4] K. Ito, K. Kabara, T. Sanai, K. Toko, Y. Imai, M. Tsunoda, and T. Suemasu, J. Appl. Phys. **116**, 053912 (2014).

[5] K. Ito, G. H. Lee, H. Akinaga, and T. Suemasu, J. Cryst. Growth **322**, 63 (2011).

[6] K. Ito, K. Harada, K. Toko, H. Akinaga, and T. Suemasu, J. Cryst. Growth **336**, 40 (2011).

[7] T. Sanai, K. Ito, K. Toko, and T. Suemasu, J. Cryst. Growth **357**, 53 (2012).

[8] K. Ito, T. Sanai, S. Zhu, Y. Yasutomi, K. Toko, S. Honda, S. Ueda, Y. Takeda, Y. Saitoh, Y. Imai, A. Kimura, and T. Suemasu, Appl. Phys. Lett. **103**, 232403 (2013).

[9] K. Ito, T. Sanai, Y. Yasutomi, S. Zhu, K. Toko, Y. Takeda, Y. Saitoh, A. Kimura, and T. Suemasu, J. Appl. Phys. **115**, 17C712 (2014).

[10] K. Kabara, M. Tsunoda, and S. Kokado, Appl. Phys. Express **7**, 063003 (2014).

[11] J. C. Wood and A. J. Nozik, Phys. Rev. B **4**, 2224 (1971).

[12] C. A. Kuhnen, R. S. de Figueiredo, V. Drago, and E. Z. da Silva, J. Magn. Magn. Mater. **111**, 95 (1992).

[13] J. L. Costa-Krämer, D. M. Borsa, J. M. García-Martín, M. S. Martín-González, D. O. Boerma, and F. Briones, Phys. Rev. B **69**, 144402 (2004).

[14] K. Mibu, M. Seto, T. Mitsui, Y. Yoda, R. Masuda, S. Kitao, Y. Kobayashi, E. Suharyadi, M. Tanaka, M. Tsunoda, H. Yanagihara, and E. Kita, Hyperfine Interact. **217**, 127 (2013).

[15] K. H. Jack, Proc. R. Soc. London A **195**, 34 (1948).

[16] P. Monachesi, T. Björkman, T. Gasche, and O. Eriksson, Phys. Rev. B **88**, 054420 (2013).

[17] A. Sakuma, J. Magn. Magn. Mater. **102**, 127 (1991).

[18] S. F. Matar, A. Houari, and M. A. Belkhir, Phys. Rev. B **75**, 245109 (2007).